ZIBELINE INTERNATIONAL™ PUBLISHING

ISSN: 2521-0890 (Print)
ISSN: 2521-0491 (Online)
CODEN: GBEEB6

Geological Behavior (GBR)

DOI: http://doi.org/10.26480/gbr.01.2025.46.52

RESEARCH ARTICLE

GRAVITY BASED MAPPING OF SEDIMENTARY THICKNESS AND STRUCTURAL TRENDS IN THE SOKOTO BASIN, NORTHWESTERN NIGERIA

Abdulmalik Shehu Sfada[a*], Abdullah Musa Ali[b]

[a] Department of Geology, School and Observatory of Earth Sciences, University of Strasbourg, Strasbourg, France.
[b] Department of Geology, Bayero University Kano, Nigeria
**Corresponding Author's Email: abdulmalik.shehu@etu.unistra.fr*

ARTICLE DETAILS

Article History:

Received 15 July 2025
Revised 23 August 2025
Accepted 28 September 2025
Available online 03 November 2025

ABSTRACT

This study presents a gravity-based investigation of sedimentary thickness and structural trends within the Sokoto Basin, Northwestern Nigeria, bounded by latitudes 13°00′N–13°30′N and longitudes 4°30′E–5°30′E. Bouguer anomaly values in the area range from 66.16 mGal to 93.08 mGal, with lower values associated with thick sedimentary cover and higher values indicating basement uplift or intrusions. The regional Bouguer anomaly map shows gravity values between 64.07 mGal and 93.77 mGal, highlighting a north–south gradient likely related to basement relief and tectonic influence. The residual Bouguer anomaly map isolates local features, with anomalies ranging from approximately -5.98 mGal to +5.65 mGal, corresponding to variations in sedimentary thickness and shallow intrusions. Spectral enhancement through upward continuation to 1 km suppressed shallow noise and emphasized deep-seated structures, while the First Vertical Derivative (FVD) map revealed tectonic trends in SW–NE, NW–SE, and N–S directions, indicating active faulting and lithologic boundaries. Structural analysis using CET lineament mapping confirmed regional fault alignments and deep-seated fractures acting as potential hydrocarbon migration pathways. Depth estimations using Source Parameter Imaging (SPI) indicated basement depths ranging from 0.931 km to 5.174 km. Power Spectral Analysis revealed two depth layers: a deeper layer (D1) with depths from 0.92 km to 5.02 km (average: 2.505 km), and a shallow layer (D2) with depths from 0.132 km to 1.178 km (average: 0.568 km). Euler Deconvolution with Structural Index (SI) = 1 yielded depths between -683 m and 5078 m, while SI = 2 gave a broader range from -832 m to 5474 m. The central-western zone near 13.2°N and 4.8°E was identified as a major sedimentary trough, marked by the deepest basement relief and highest sediment accumulation. These findings underscore the Sokoto Basin's resource potential and demonstrate the utility of gravity methods in characterizing sedimentary basins.

KEYWORDS

Sokoto Basin, Gravity Data, Sedimentary Thickness, Euler Deconvolution, Source Parameter Imaging (SPI), Spectral Analysis.

1. INTRODUCTION

The Sokoto Basin, located in the northwestern part of Nigeria, constitutes the southeastern sector of the extensive Iullemmeden Basin, which stretches across several West African countries. The basin is characterized by a thick sequence of Cretaceous to Tertiary sedimentary rocks unconformably overlying the Precambrian basement complex (Kogbe, 1989; Obaje, 2009). Owing to its geotectonic setting and stratigraphic complexity, the basin holds significant potential for hydrocarbons, groundwater, and mineral resources. However, despite several geological investigations, the internal structural framework and distribution of sedimentary thickness, especially within the Dinawa region remain poorly defined due to limited high-resolution geophysical constraints.

Gravity methods offer a robust and cost-effective means of imaging subsurface density variations, particularly in sedimentary environments where drilling data are sparse. Bouguer gravity anomalies are sensitive to lateral density contrasts and can reveal important subsurface features, including faults, intrusive bodies, and variations in sedimentary thickness (Telford et al., 1990; Blakely, 1995; Musa et al., 2024; Shuaibu et al., 2025). The effectiveness of gravity data is further enhanced through the application of derivative filters such as the First Vertical Derivative (FVD), upward continuation, and regional-residual separation techniques, which improve the resolution of both shallow and deep-seated structures (Fairhead and Okereke, 1987; Awoyemi and Hammed, 2016).

Numerous studies have demonstrated the applicability of gravity data for structural and sedimentary basin analysis in Nigeria. For instance, a group researcher employed gravity-based techniques to delineate basement topography and fault systems in parts of the Sokoto and Chad Basins (Adamu et al., 2021; 2022). A group researchers further highlighted the role of gravity-derived lineament mapping in identifying fault-controlled sediment accumulation zones and potential hydrocarbon traps (Salako, 2014; Emujakporue and Ofoha, 2015). These studies underscore the value of gravity data interpretation in unraveling complex subsurface frameworks, especially in underexplored basins. This study aims to map sedimentary thickness and delineate structural trends within the Sokoto Basin using gravity data obtained from the Earth Topography Gravity Model (ETOPG1). Processing techniques such as Bouguer anomaly mapping, upward continuation at 1 km, FVD filtering, and residual separation were applied using Oasis Montaj software. Depth estimation techniques including Source Parameter Imaging (SPI), power spectral analysis, and Euler Deconvolution were employed to determine the depth to the basement and define subsurface geometries.

Quick Response Code	Access this article online	
	Website: www.geologicalbehavior.com	DOI: 10.26480/gbr.01.2025.46.52

Cite The Article: Abdulmalik Shehu Sfada, Abdullah Musa Ali (2025). Gravity Based Mapping Of Sedimentary Thickness And Structural Trends In The Sokoto Basin, Northwestern Nigeria. *Geological Behaviour (GBR)* 9(1): 46-52.

2. Geology And Location Of The Study Area

The Sokoto Basin, a southeastern extension of the Iullemmeden Basin, spans parts of Sokoto, Zamfara, and Kebbi States in northwestern Nigeria (Obaje et al., 2013). It forms part of Nigeria's inland basins linked to Cretaceous rifting during the opening of the South Atlantic Ocean (Obaje et al., 2019). The basin is characterized by low-relief topography (250–400m meters above sea level), punctuated by features like the Dange Scarp, which reflects subsurface structural controls (Hamza and Garba, 2009). Stratigraphically, the basin comprises a sequence from the Illo and Gundumi Formations at the base to the Gwandu Formation at the top, thickening northwestward toward the Niger border (Obaje et al., 2013). It hosts petroleum system elements, including source rocks in the Dukamaje Formation, reservoir sandstones, and regional seals such as the Gamba and Gwandu shales (Obaje et al., 2019). Structural features such as folds and faults are prominent along the Goronyo–Taloka axis, indicating tectonic activity relevant for hydrocarbon trapping.

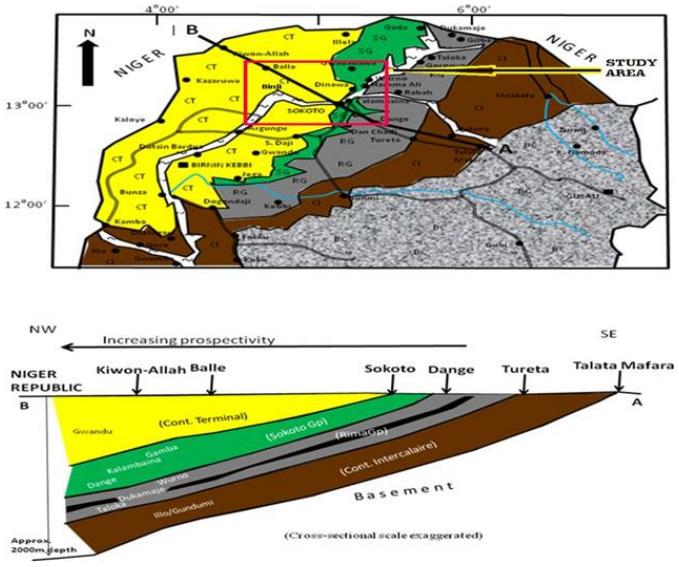

Figure 1: Geological Map of the Sokoto Basin showing the Study area (Obaje et al., 2019).

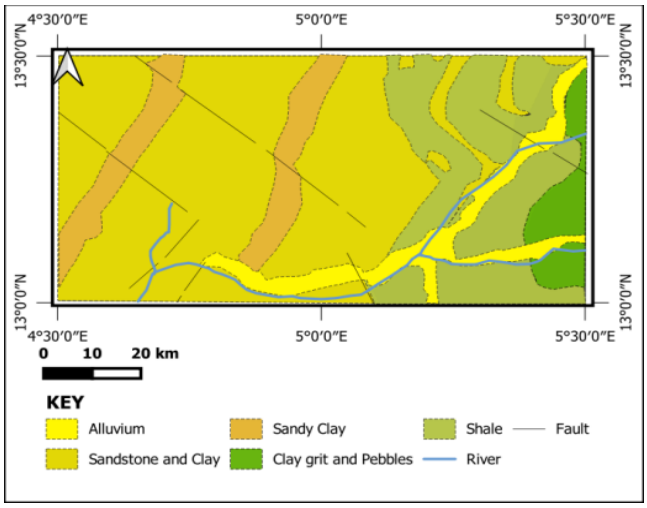

Figure 2: Geological map of the study area (after NGSA, 2020)

The map (figure 2) presents the geological framework of the study area located in the northwestern Sokoto Basin, bounded by latitudes 13°00′N–13°30′N and longitudes 4°30′E–5°30′E, covering approximately 6,180 km^2. It displays a variety of surface lithologies including alluvium, sandstone and clay, sandy clay, shale, and clay grit with pebbles. Sandstone and clay units dominate the central region, while sandy clay and alluvium are distributed along the western and riverine zones. The northeastern and southeastern parts are characterized by shale and clay-rich units with pebbles, indicating fluvial to shallow marine depositional environments. River systems, shown in blue, align with low-lying zones and finer sediment deposits. Structurally, the map reveals fault lines trending in NE–SW and NW–SE directions, suggesting tectonic activity and structural deformation within the basin (NGSA, 2020).

3. Materials And Methods

This study integrates geological field mapping with gravity data analysis to delineate subsurface structures and estimate basement depth in the Dinawa area, Sokoto Basin. The approach combined surface observations with processed gravity anomalies for improved subsurface interpretation.

3.1 Materials

Field mapping utilized GPS, compass-clinometer, geological hammer, topographic maps, hand lens, and sample bags for lithological and structural documentation. Gravity data were sourced from the ETOPG1 model (1' × 1'), which incorporates WGM 2012 and EGM 2008 (Balmino et al., 2011; Zelalem et al., 2018). Data processing employed Oasis Montaj 8.4, QGIS 3.30, Surfer 16, and Microsoft Excel.

3.2 Geological Field Mapping

A total area of ~6,185 km^2 was covered through reconnaissance and detailed mapping. Outcrop descriptions, lithologic boundaries, and structural measurements (strike/dip, joints, fractures) were recorded and georeferenced using GPS.

3.3 Geophysical Data Processing

Bouguer gravity data were gridded using the minimum curvature method. Reduction to the Equator (RTE) was applied due to the region's low magnetic latitude. To enhance deep features and reduce surface noise, upward continuation at 1 km was performed. Residual anomalies were obtained via first-order polynomial regional removal. The First Vertical Derivative (1VD) was applied to highlight shallow structures and contacts.

3.3.1 Depth Estimation

Subsurface depths were estimated using:

- Source Parameter Imaging (SPI) to assess magnetic source depths.
- Euler Deconvolution (structural indices SI = 1 and 2) for depth and geometry of subsurface bodies (Reid et al., 2003).
- Power Spectral analysis

3.3.2 Analytical Approach

Qualitative interpretation involved structural trend analysis from filtered maps, while quantitative methods included SPI and Euler solutions. Results were cross-validated and interpreted in conjunction with field data to better understand basin structure and potential resource zones (Adamu et al., 2022; Abdelhakim et al., 2021).

4. Result

4.1 Potential Maps of the study area

The Bouguer anomaly values in the study area vary from 66.16 mGal to 93.08 mGal (Figure 3), lower Bouguer values indicate sedimentary infill where high Bouguer portions indicate possible intrusion of the basement to sediment overburden. The colour legend bar distinguishes regions of high gravity (red and pink), corresponding to areas with high-density contrasts beneath the surface; intermediate values (green and yellow); and gravity lows (blue), indicating regions with low-density contrast.

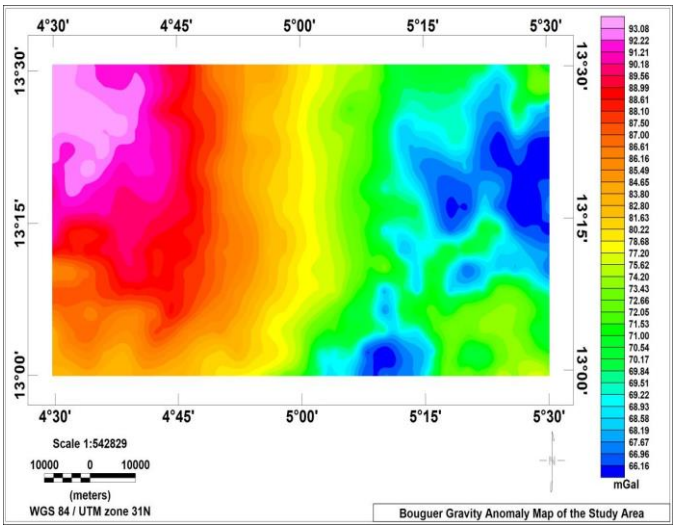

Figure 3: Bouguer Anomaly Map of the Study Area

The regional Bouguer anomaly map (Figure 4) shows values ranging from 64.07 mGal to 93.77 mGal, with a decrease from north to south. This gradient might indicate the degree of igneous intrusion of the basement rocks, with more extensive intrusions in the northern part of the research area compared to the southern part.

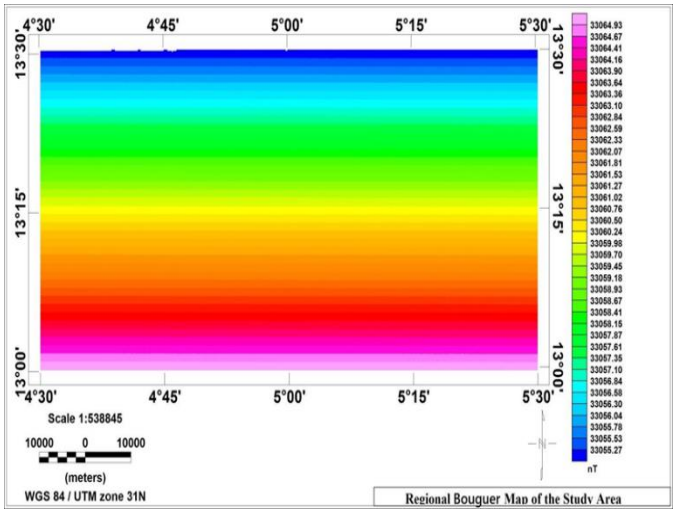

Figure 4: Regional Magnetic Field Map of the Study Area

The Residual Bouguer anomaly map illustrated in Figure 5 indicates a high maximum anomaly value of approximately 5.65 mGal in the northeastern and southeastern regions of the study area, along with minimum anomaly value of around -5.98 mGal in the northwestern, southwestern, and deeper southeastern edge. These zones of high Bouguer anomalies might result from shallow intrusions. Mostly, negative gravity anomalies are associated with less dense formations, such as thick sedimentary sections in these areas (Adamu et al., 2022)

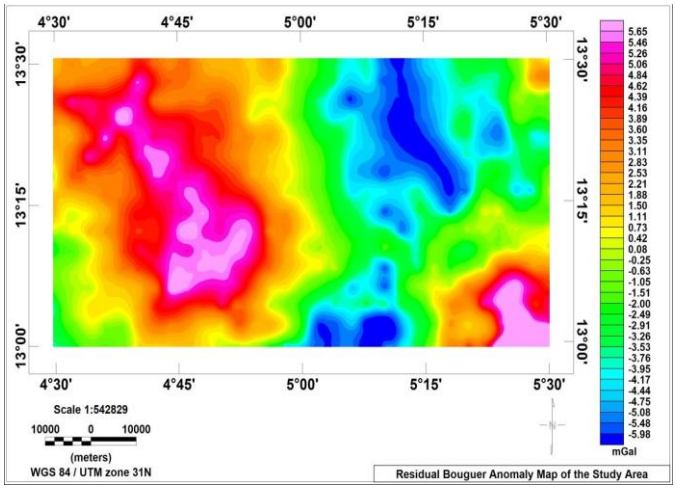

Figure 5: Residual Bouguer Map of the study area

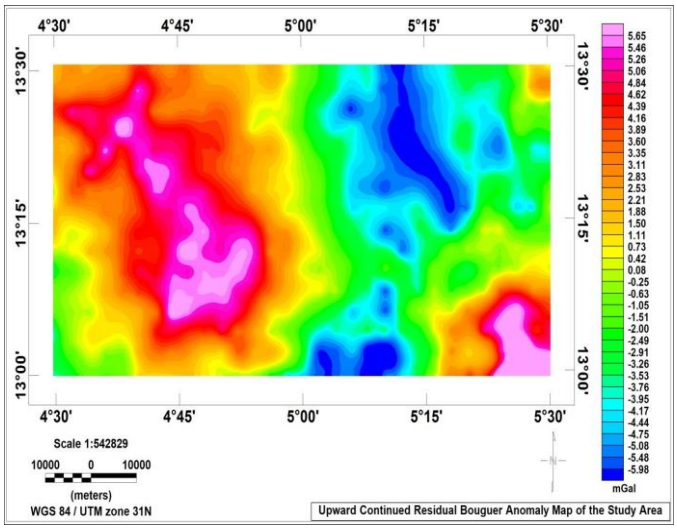

Figure 6: Upward Continued Map of the study area

To reduce the interference of surface noise, the Bouguer anomaly map was upward continued by 1 km, as displayed in Figure 6.

4.2 Edge Detection Techniques

4.2.1 First Vertical Derivative

The First Vertical Derivative (FVD) was utilized to highlight shallow geological features and delineate geologic boundaries using the Step by Step Filter on the MAGMAP tool in Oasis Montaj software.

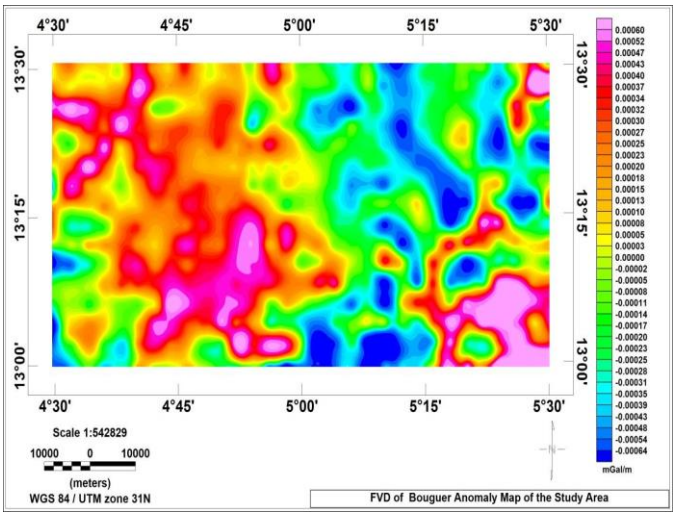

Figure 7: First Vertical Derivative (FVD) Map of Bouguer Anomaly of the Study Area

As illustrated in Figure 7, the FVD map of the Bouguer data can be divided into three zones, with most causative structures trending SW-NE, NW-SE, and a few trending N-S. The highly sedimentary fill with low gravity anomalies is evenly distributed across the map. The FVD map shows shallow features with high gravity anomalies, which are prominent in the southwestern and northwestern parts of the research area. Additionally, the FVD shows zones of shallow features with low gravity anomalies, predominantly in the northeastern and some part of the southeastern research area. Zones exhibit a sharp contrast between pink and blue, indicating high- and low-density contrasts, which may suggest sedimentary fill along the contact zones of intruded structures.

4.2.2 Lineaments Extraction

The lineaments of the study area were extracted using the CET analysis tool of the Oasis Montaj software to extract the ridge/valley structures in the region and was further superimposed on the First Vertical Derivative of the maps deduced using the MAGMAP tools by applying the line path on the map tools of the Oasis Montaj to relate the obtained features directly with their derived sources.

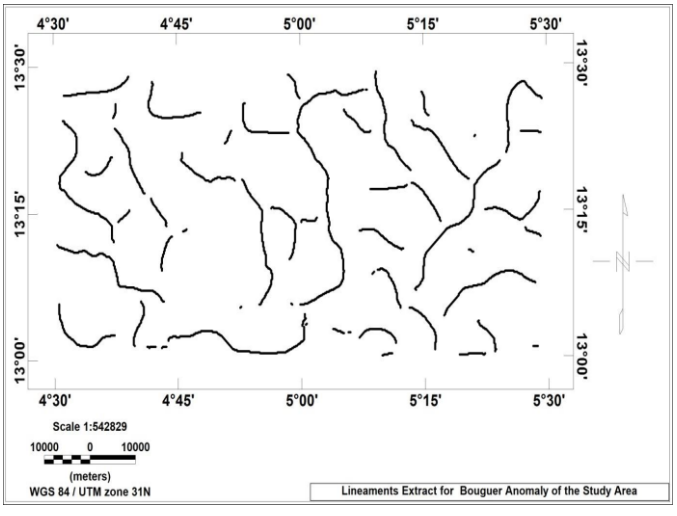

Figure 8: Bouguer Lineaments Map of the Study Area.

The structural trend derived from the gravity data in (Figure 8) of the study area revealed structures consistent with the geology of the research area (Figure 7), trending SW-NE, NW-SE, and few N-S. The trend lines correspond to likely boundaries between geological formations, with longer lines indicating major contacts between geologic structures of

varying compositions. The fault zones shown in this map primarily align with tectonically derived faults along valleys. These lineaments represent faults and fractures, likely associated with sub-basins, magmatic intrusions, tectonic movements, or metamorphism. The longer lines indicate major faults.

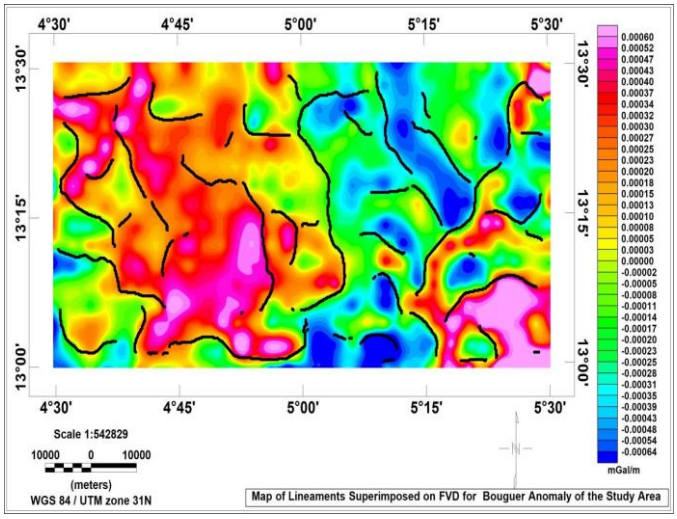

Figure 9: Map of Bouguer lineaments Superimposed on its First Vertical Derivative

The overlay of the lineaments on the FVD map (Figure 7) delineates the locations of potential boundaries of valleys and ridges and for other various geologic structures in the subsurface. This overlay clearly defines the edges surrounding the geologic structures. These lineaments could serve as favorable pathways for controlling hydrocarbon accumulation, hydrogeology, mineral deposits, and geothermal fluid circulation in the area. A study asserted that lineament patterns are favorable structural conditions for controlling various hydrocarbon deposits in the Niger Delta Basin (Emujakporue and Ofoha, 2015).

4.3 Depth Estimation

Similar to the aeromagnetic data, three methods were used to estimate the depth to basement from the gravity data to evaluate the depth to Bouguer sources: Source Parameter Imaging (SPI), power spectral analysis and Standard Euler deconvolution. The results are discussed below

4.3.1 Source Parameter Imaging

The depth to the basement was estimated using Source Parameter Imaging (SPI) from the Bouguer anomaly map, as shown in Figure 10. The depths range from a minimum of 0.931km, indicated by dark blue colour, to a maximum of 5.174km indicated by deep pink colour. The map reveals that the southeastern, northeastern, southwestern, and northwestern parts of the study area have significant SPI depths, typically greater than 3.667km

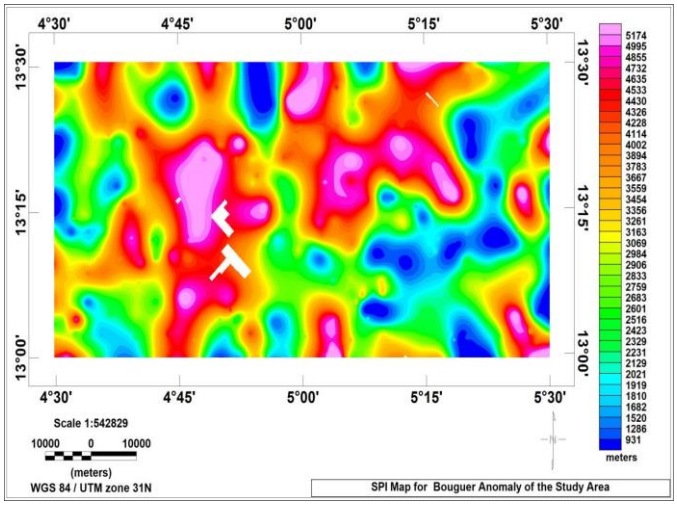

Figure 10: SPI Depth Map from Bouguer data of the Study Area.

4.3.2 Spectral Analysis Depth Estimation

The power spectral depth analysis of Bouguer data reveals that the depth to the deeper layer (D1) in the study area varies from 0.92km to 5.02km, with an average depth of 2.505km. The depth to the shallow layer (D2) ranges from 0.132km to 1.178km, with an average depth of 0.568km, as displayed in Table 1.

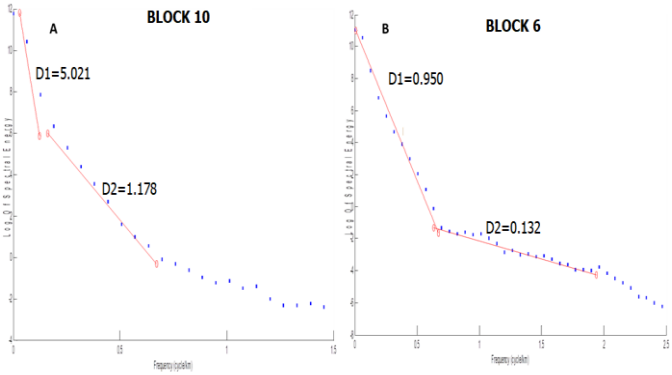

Figure 11: Spectral Plot of Block 10 and 6 (example from 21 subdivided blocks of Bouguer data)

Table 1: Spectral Estimates depth to the Bouguer Source Layers of the study area

S/No	Block	Coordinates	D1	D2
1	1	13⁰ 22'30"N / 4⁰ 37'30"E	2.230	0.762
2	2	13⁰ '22'30'N / 4⁰ 45'00"E	2.740	0.601
3	3	13⁰ 22'30"N / 4⁰ 52'30"E	3.145	0.879
4	4	13⁰ 22'30"N / 5⁰ 00'00"E	3.140	0.804
5	5	13⁰ 22'30"N / 5⁰ 07'30"E	2.230	0.339
6	6	13⁰ 22'30"N / 5⁰ 15'00"E	0.930	0.132
7	7	13⁰ 22'30"N / 5⁰ 22'30"E	0.970	0.326
8	8	13⁰ 15'00"N / 4⁰ 37'30"E	1.131	0.308
9	9	13⁰ 15'00"N / 4⁰ 45'00"E	4.843	1.091
10	10	13⁰ 15'00"N / 4⁰ 52'30"E	5.021	1.178
11	11	13⁰ 15'00"N / 5⁰ 00'00"E	4.870	1.027
12	12	13⁰ 15'00"N / 5⁰ 07'30"E	1.580	0.243
13	13	13⁰ 15'00"N / 5⁰ 15'00"E	0.920	0.179
14	14	13⁰ 15'00"N / 5⁰ 22'30"E	0.981	0.249
15	15	13⁰ 07'30"N / 4⁰ 37'30"E	2.250	0.586
16	16	13⁰ 07'30"N / 4⁰ 45'00"E	5.007	1.153
17	17	13⁰ 07'30"N / 4⁰ 52'30"E	4.398	0.905
18	18	13⁰ 07'30"N / 5⁰ 00'00"E	2.310	0.245
19	19	13⁰ 07'30"N / 5⁰ 07'30"E	0.980	0.186
20	20	13⁰ 07'30"N / 5⁰ 15'00"E	0.950	0.262
21	21	13⁰ 07'30"N / 5⁰ 22'30"E	1.970	0.469

Figure 12 deeper depth layer contour map of the study area reveals significant subsurface variation, with depths ranging from approximately 0.5 km to over 5.1 km. The central-western portion of the map, particularly around coordinates 13.2°N and 4.8°E, displays the deepest basement

depths, indicating the presence of a major sedimentary trough or structural depression, likely associated with thick sediment accumulation. In contrast, the eastern and southwestern margins exhibit relatively shallower basement depths, suggesting the presence of uplifted basement blocks or structural highs. The concentration of contour lines in certain regions also reflects steep depth gradients, which may correspond to fault zones or tectonic boundaries. This spatial variation in depth is critical for understanding the basin architecture and could guide further exploration for geothermal or hydrocarbon resources.

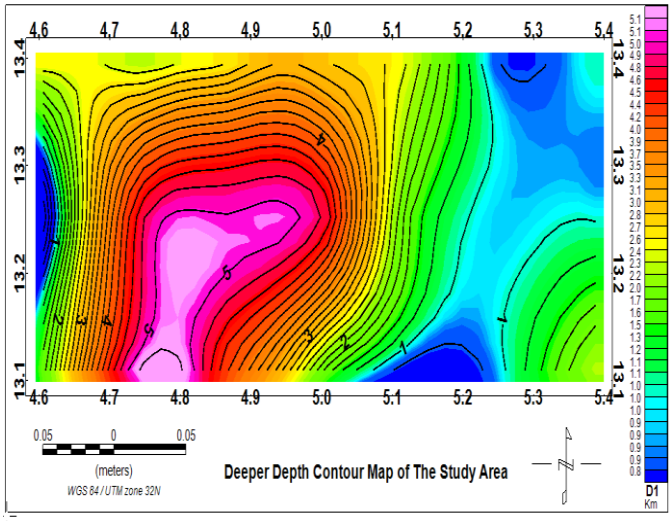

Figure 12: Deeper Depth Contour Map of the Study Area

Shallow Depth Layer Contour of, Figure 13. It shows basement depths ranging from approximately 0.1 km to 1.2 km, with the shallowest areas concentrated around the eastern and southwestern portions of the map. The deepest part of the shallow layer, shown in pink to white tones, appears centered near 13.2°N and 4.8°E, aligning with the deeper zone seen in the previous map. This distribution reflects near-surface geological structures and could indicate regions of recent sediment deposition or uplifted basement blocks.

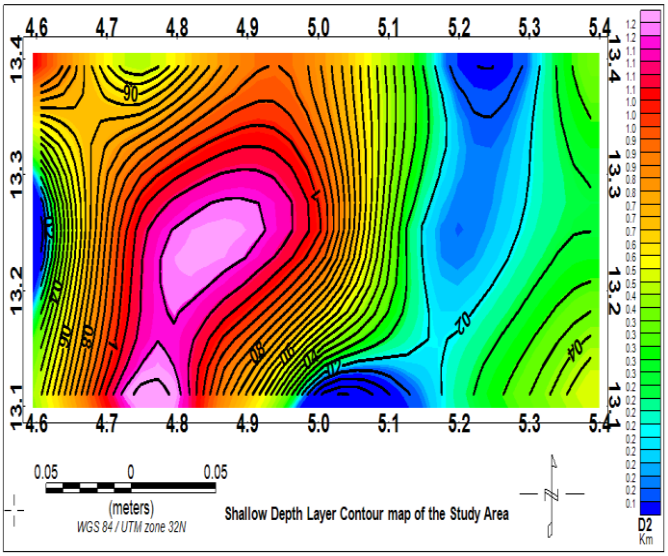

Figure 13: Shallow Depth layer Map of the Study Area

4.3.3 Standard Euler Deconvolution Depth

Two Euler deconvolution maps were generated for the Bouguer gravity data. The Euler depths were estimated using vertical derivatives in three dimensions (x, y, and z). Vertical derivatives enhance shallow Bouguer anomalies. Hence, depths of shallow Bouguer anomalies for different structural indices are displayed by Euler method. In this study, Two Euler maps were generated from the Bouguer Map for three different structural indexes (1, 2) as shown in (Figure 14 and 15). The areas in the maps without specific gravity signatures or colour indicate that there is no Euler solution (depth) for the particular structural index used. Blue colour shows deep lying density bodies while the pink colour shows shallow density bodies. Euler solution for dyke and sills as source (structural index =1), revealed depths ranging from - 683m to 5078m. Clustering solutions were seen to occur all over the map (Figure 14).

However, maximum depths ranging from 4015m to 5078m were observed in southwestern, southeastern and centre part of the study area, fault and lineament trending WSW- ENE, NE-SW and NNW-SSE directions as shown in (Figure 12). This gives an insight to the approximate depth range of all the lineaments/ fractures. Euler solution for Horizontal cylinder and pipe (structural index = 2), revealed depths ranging from -832m to 5474m. Clustering solutions were seen to occur all over the map (Figure 15). However, maximum depths ranging from 4582m to 5474m were observed in in southwestern, eastern and northwestern part of the study area.

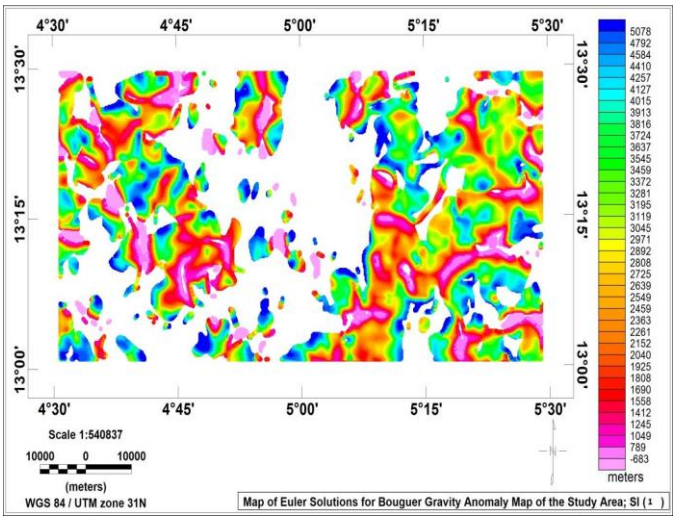

Figure 14: Euler deconvolution for Bouguer map for SI= 1

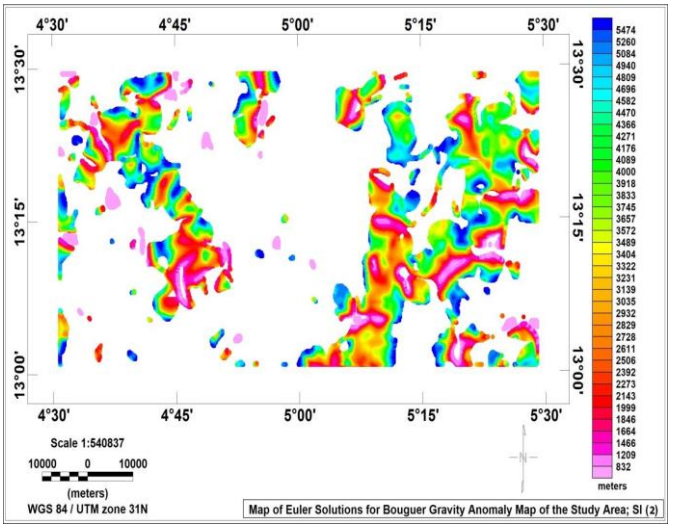

Figure 15: Euler deconvolution for Bouguer map for SI= 2

5. Discussion Of Results

The gravity data analysis over the study area provides critical insights into the subsurface structures, lithologic variations, and sedimentary basin architecture. The Bouguer anomaly map (Figure 3) reveals significant gravity variation across the area, with values ranging from 66.16 mGal to 93.08 mGal. The relatively low Bouguer values are characteristic of sedimentary infill, whereas the higher values indicate possible basement intrusions into the sedimentary overburden. The colour legend reflects these variations, with red and pink denoting high-density contrasts, green to yellow representing intermediate densities, and blue indicating low-density regions. These variations are associated with differential density distributions related to sedimentary thickness and crystalline basement exposures.

The regional Bouguer anomaly map (Figure 4), with values between 64.07 mGal and 93.77 mGal, shows a north-south gravity gradient, which may correspond to variations in basement topography or igneous intrusions. The higher gravity in the northern region suggests more extensive basement intrusions or uplift, consistent with tectonic activities influencing the area. The residual Bouguer anomaly map (Figure 5) isolates local anomalies by removing the regional trend. The map displays maximum positive anomalies (~5.65 mGal) in the northeastern and southeastern regions, possibly indicating shallow intrusions, and minimum anomalies (~ -5.98 mGal) in the northwestern and

southwestern regions, which likely correspond to thicker sedimentary sequences (Adamu et al., 2021; Adamu et al., 2022). These low-density anomalies suggest areas of potential hydrocarbon accumulation, as thick sedimentary basins are typically favorable for petroleum systems.

To suppress near-surface noise and enhance deeper geological features, an upward continuation to 1 km was applied to the Bouguer data (Figure 6). This transformation smooths shallow sources and enhances the influence of deep-seated structures, further validating the presence of regional basement trends and deep faults. The First Vertical Derivative (FVD) map (Figure 7) highlights shallow geological boundaries and structural edges. Predominant SW–NE, NW–SE, and localized N–S trends were observed, corresponding to known tectonic directions in the basin. Zones of high gravity contrast (e.g., sharp pink-to-blue transitions) likely reflect contacts between intrusions and sedimentary units. These features are critical for delineating geologic boundaries, particularly in hydrocarbon and geothermal exploration.

Lineament extraction using CET analysis and its superposition on the FVD map (Figure 8) provided further structural insights. The observed structural trends align well with regional tectonic settings, revealing major fault systems and fracture networks that trend predominantly SW–NE, NW–SE, and N–S. These lineaments, particularly the longer ones, are likely associated with deep-seated faults, which could act as migration pathways for fluids, traps for hydrocarbons, or zones of mineralization. The interpretation aligns with who suggested that such lineament patterns play a key role in controlling fluid movement and hydrocarbon entrapment in sedimentary basins (Emujakporue and Ofoha, 2015). In terms of depth estimation, three techniques Source Parameter Imaging (SPI), Power Spectral Analysis, and Standard Euler Deconvolution were applied to characterize basement relief and intrasedimentary features.

The SPI map (Figure 10) estimated depths ranging from 0.931 km to 5.174 km, with greater depths (>3.6 km) observed in the southwestern, southeastern, and northeastern regions. These variations suggest significant sedimentary thickness, possibly controlled by fault-bounded sub-basins or tectonic depressions. The Power Spectral Analysis revealed a deeper layer (D1) at depths of 0.92 km to 5.02 km (average 2.505 km), and a shallow layer (D2) at depths ranging 0.132 km to 1.178 km (average 0.568 km). The results confirm a bimodal depth distribution, with shallow anomalies likely caused by tectonic uplift or shallow intrusions, and deeper sources attributable to variations in basement composition and deformation, including faulting and fracturing.

The Euler Deconvolution method further refined the depth estimations and structural interpretations. For Structural Index (SI) = 1 (dykes and sills), depths ranged from -683 m to 5078 m, with notable clustering in the southwestern and central zones (Figure 14). These clusters coincide with mapped faults and lineaments, suggesting possible intrusions along tectonic boundaries. For SI = 2 (horizontal cylinders and pipes), depths varied from -832 m to 5474 m, with maximum depths in the eastern and northwestern regions (Figure 15). These depth distributions reflect multi-episode deformation and basement complexity, confirming the presence of both shallow and deep structural features across the study area. The shallow depth layer contour map illustrates the near-surface structural configuration of the study area, with depths ranging from approximately 0.1 to 1.2 km.

The central portion, particularly around 13.2°N and 4.8°E, reveals the highest values, indicating relatively deeper zones within the shallow layer, while the eastern and southwestern regions show shallower depths. This suggests localized subsidence or sediment accumulation in the central zone, possibly overlying a deeper structural depression. The close spacing of contours indicates sharp depth variations, likely related to faulting or lithological boundaries. Overall, the map reflects the surface expression of deeper geological controls observed in the previous depth layer. Figure 14 shows notable subsurface depth variation, with basement depths ranging from about 0.5 km to over 5.1 km. The deepest part, located in the central-western section near 13.2°N and 4.8°E, suggests a significant sedimentary trough or structural low, likely linked to extensive sediment accumulation. Shallower depths along the eastern and southwestern margins point to uplifted basement structures. The dense contour spacing in parts of the map indicates steep gradients, possibly marking faulted or tectonically active zones. These variations provide insight into the structural framework of the basin and highlight zones of interest for further resource exploration.

6. Conclusion

The gravity-based geophysical analysis of the Sokoto Basin (13°00′N–13°30′N and 4°30′E–5°30′E) has provided critical insights into subsurface structural configurations, sedimentary fill, and tectonic architecture. Bouguer anomaly values from 66.16 to 93.08 mGal reveal contrasting densities between basement and sedimentary units, while regional values between 64.07 and 93.77 mGal support interpretations of broad crustal variation. The residual anomalies, ranging from -5.98 mGal to +5.65 mGal, reflect localized features such as intrusions and thick sediment accumulations. Spectral filtering techniques including 1 km upward continuation and FVD mapping clarified deeper geological trends and enhanced structural interpretations, confirming fault-aligned density contrasts trending SW–NE, NW–SE, and N–S. CET-based lineament mapping validated these orientations and identified key fault systems that likely influence basin development and fluid migration. Depth estimation results further support a complex, multi-depth subsurface system. SPI analysis estimated depths between 0.931 km and 5.174 km, indicating significant sedimentary thickness in fault-controlled depressions. Power Spectral Analysis reinforced this, identifying a deeper layer (D1) from 0.92 km to 5.02 km and a shallow layer (D2) from 0.132 km to 1.178 km. Euler Deconvolution with SI = 1 showed depths between -683 m and 5078 m, and with SI = 2 from -832 m to 5474 m, highlighting both shallow and deep structural features. The central-western zone around 13.2°N and 4.8°E emerged as a major trough, suggesting tectonic subsidence and sediment accumulation. These geophysical results confirm that the Sokoto Basin contains favorable conditions for hydrocarbon and geothermal exploration. This study demonstrates the effectiveness of integrated gravity techniques in resolving basement topography and sedimentary configuration in complex continental basins.

Conflicts Of Interest

The authors declare that they have no known competing financial interests or personal relationships that could have appeared to influence the work reported in this article.

References

Adamu, A.A., Ayuba, I.A., and Abdulkarim, A.A., 2021. Structural interpretation and depth estimation using gravity data in Sokoto Basin, Northwestern Nigeria. Arabian Journal of Geosciences, 14 (6), Pp. 1–14.

Adamu, A.A., Ayuba, I.A., and Yusuf, K.A., 2022. Basement depth evaluation and structural mapping using gravity data in part of Chad Basin, Nigeria. SN Applied Sciences, 4 (3), Pp. 1–17.

Awoyemi, M.O., and Hammed, O.S., 2016. Integration of magnetic and electrical resistivity methods in geological mapping of basement complex terrain in Southwestern Nigeria. Nigerian Journal of Technological Development, 13 (2), Pp. 53–59.

Balmino, G., Vales, N., Bonvalot, S., and Briais, A., 2011. Spherical harmonic modeling to ultra-high degree of Bouguer and isostatic anomalies. Journal of Geodesy, 86, Pp. 499–520.

Blakely, R.J., 1995. Potential theory in gravity and magnetic applications. Cambridge University Press.

Emujakporue, G.O., and Ofoha, C.G., 2015. Gravity interpretation and lineament analysis in the Niger Delta Basin. Journal of Applied Geology and Geophysics, 3 (5), Pp. 1–8.

Fairhead, J.D., and Okereke, C.S., 1987. A regional gravity study of the West African Rift System in Nigeria and Cameroon and its tectonic interpretation. Tectonophysics, 143 (1–3), Pp. 141–159.

Hamza, H., and Garba, I., 2009. Geological evolution and hydrocarbon potential of the Sokoto Basin, northwestern Nigeria. Journal of Mining and Geology, 45 (1), Pp. 33–43.

Kogbe, C.A., 1989. Geology of Nigeria (2nd ed.). Rock View (Nigeria) Ltd.

Musa, A.A., Shehu, A., and Lawan, A.Y., 2024. Validating the accuracy of natural electric field (NEF) water detectors for hydrogeophysical exploration. International Journal of Energy and Water Resources, 9 (12). https://doi.org/10.1007/s42108-024-00307-x

NGSA. 2020. Geological map of Nigeria. Nigerian Geological Survey Agency.

Obaje, N.G., 2009. Geology and mineral resources of Nigeria. Springer.

Obaje, N.G., Abaa, S.I., Agyingi, C.M., and Umar, M., 2019. Sedimentology and stratigraphy of Cretaceous–Tertiary sequences in Sokoto Basin. Journal of Petroleum Geology, 42 (4), Pp. 459–473. https://doi.org/10.1111/jpg.12718

Obaje, N.G., Abaa, S.I., Najime, T., and Abubakar, M.B., 2013. Stratigraphy, paleoenvironment and hydrocarbon resource potentials of the Sokoto Basin, NW Nigeria. Journal of African Earth Sciences, 73, Pp. 1–11. https://doi.org/10.1016/j.jafrearsci.2012.08.011

Obaje, N.G., Najime, T., and Adamu, M., 2020. Hydrocarbon resource evaluation in the Sokoto Basin, NW Nigeria. Journal of African Earth Sciences, 171, Pp. 103964.

Ofoegbu, C.O., Onuoha, K.M., and Anakwuba, E.K., 1987. Spectral analysis of aeromagnetic data over the middle Benue Trough of Nigeria. Geophysical Journal International, 90 (2), Pp. 373–386.

Reid, A.B., Allsop, J.M., Granser, H., Millett, A.J., and Somerton, I.W., 1990. Magnetic interpretation in three dimensions using Euler deconvolution. Geophysics, 55 (1), Pp. 80–91.

Salako, K.A., 2014. Structural interpretation using high-resolution aeromagnetic data over part of the Dahomey Basin, southwestern Nigeria. International Journal of Geosciences, 5 (8), Pp. 790–801.

Shuaibu, A.M., Shehu, S.A., and Okiyi, I.M., 2025. Application of geo-electrical techniques for groundwater potential delineation in Mashiji and its environ, Malumfashi, Northwest Nigeria. Pakistan Journal of Geology, 9 (1), P. 12–19.

Spector, A., and Grant, F.S., 1970. Statistical models for interpreting aeromagnetic data. Geophysics, 35 (2), Pp. 293–302.

Telford, W.M., Geldart, L.P., Sheriff, R.E., and Keys, D.A., 1990. Applied geophysics (2nd ed.). Cambridge University Press.

Thompson, D.T., 1982. EULDPH: A new technique for making computer-assisted depth estimates from magnetic data. Geophysics, 47 (1), Pp. 31–37.

Thurston, J.B., and Smith, R.S., 1997. Automatic conversion of magnetic data to depth, dip, and susceptibility contrast using the SPI method. Geophysics, 62 (3), Pp. 807–813.

Udensi, E.E., Osazuwa, I.B., and Momoh, M., 2004. Spectral analysis of aeromagnetic data and estimation of basement depths in parts of the upper Benue Trough and adjacent areas of Nigeria. Journal of Mining and Geology, 40 (2), Pp. 95–100.

Whitehead, N.E., and Musselman, H.E., 2005. Application of Euler deconvolution method to gravity data. Geophysics, 70 (6), Pp. L47–L53. https://doi.org/10.1190/1.2122411

Zelalem, A., Abdelsalam, M.G., and Mohammed, M. U., 2018. Gravity-based crustal structure of the Ethiopian Plateau. Journal of African Earth Sciences, 142, Pp. 187–198.